JOURNAL OF SPACECRAFT AND ROCKETS
Vol. 29, No. 1, January-February 1992

Multizonal Navier-Stokes Solutions for the Multibody Space Shuttle Configuration

C. L. Chen,* S. Ramakrishnan,* and K. Y. Szema*
Rockwell International Science Center, Thousand Oaks, California 91360
and
H. S. Dresser* and K. Rajagopal*
Rockwell International Space Division, Downey, California 90241

Numerical simulation of flow past the multibody Shuttle configuration in ascent mode has been carried out using the USA (unified solution algorithms) code, which is a finite volume, unified time/space marching, zonal, Reynolds-averaged Navier-Stokes solver featuring an implicit, upwind-biased scheme and total variation diminishing discretization for high accuracy. Body conforming elliptic multizonal grids were used in the computation. The agreement between computed and experimental results is reasonable. The interference effects of various components on the surface pressure distribution are discussed. The results show the importance of ensuring simulation of proper blockages due to various components of the mated Space Shuttle vehicle to obtain a reliable prediction of aerodynamic forces. Agreement between computed and experimental results could be improved by refining the definition of various geometric features and by including all geometric complexities.

Introduction

THE objective of this paper is to report results from a numerical computation of viscous flow past the multibody Shuttle [integrated Orbiter, solid rocket boosters (SRBs), and external tank (ET)] configuration in ascent mode and to emphasize the usefulness of computational fluid dynamics (CFD) in the prediction of aerodynamic loads on complex geometries. In the past, data obtained from analysis, wind-tunnel experiments, and flight tests have been used extensively to predict the aerodynamic loads for the mated Space Shuttle vehicle. Wind-tunnel data suffer from inadequacies due to scaling and wind-tunnel wall interference effects. Reliable detailed flight test data are difficult to obtain. Therefore, it appears to be a worthwhile exercise to perform numerical simulations of flow past the multibody Shuttle configuration in order to explore the possibility of generating a reliable data base for this configuration.

Numerical simulation of flow past the multibody Shuttle configuration has been reported in the literature by other researchers.[1-3] Szema et al.[1,2] obtained zonal Euler solutions for various supersonic flight conditions. NASA Ames Space Shuttle Flow Simulation Group[3] used the partial flux-splitting method with the chimera overset-grid approach[4] to solve the thin-layer Navier-Stokes equations. In this paper, we present an application of the multizonal gridding procedure for the Euler equations presented in Refs. 1 and 2 to solve the Reynolds-averaged Navier-Stokes (RANS) equations, since viscous effects may be important within the gaps of the Orbiter, the external tank, and the solid rocket booster. The multizonal gridding procedure (MZGP)[5] has some advantages over the chimera composite grid approach.[4] By ensuring continuity of grid lines across zonal boundaries, the tedious interpolation process that leads to some inaccuracies is completely avoided. The absence of lengthy bookkeeping that is a part of the chimera scheme deserves special mention. The MZGP retains the main feature of the chimera scheme, namely, the ease of handling multiple body configurations. Unlike the chimera scheme, in the case of MZGP grid lines in each zone cannot be developed independently. This may prove to be disadvantageous in some cases. Under the patching-type multizonal approach, Roe's approximate Riemann solver with slope limiter is used in all directions, avoiding the explicit specification of dissipation in the crossflow direction that is required for the partial flux-splitting method. It also predicts better boundary-layer quantities than standard flux-splitting methods.

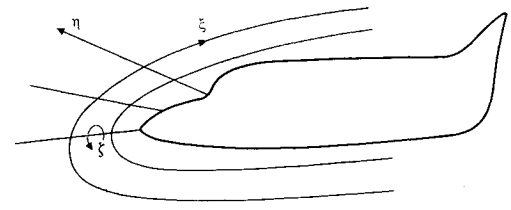

a) Orbiter alone

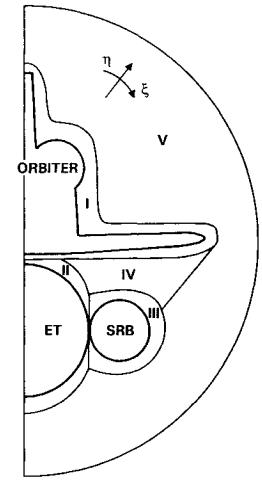

b) Multi-body Shuttle cross section

Fig. 1 Zonal topology for Orbiter alone and multibody Shuttle cross section.

Presented as Paper 90-0434 at the AIAA 28th Aerospace Sciences Meeting, Reno, NV, Jan. 8-11, 1990; received Jan. 20, 1990; revision received Aug. 21, 1990; accepted for publication Aug. 30, 1990.

*Member Technical Staff. Member AIAA.

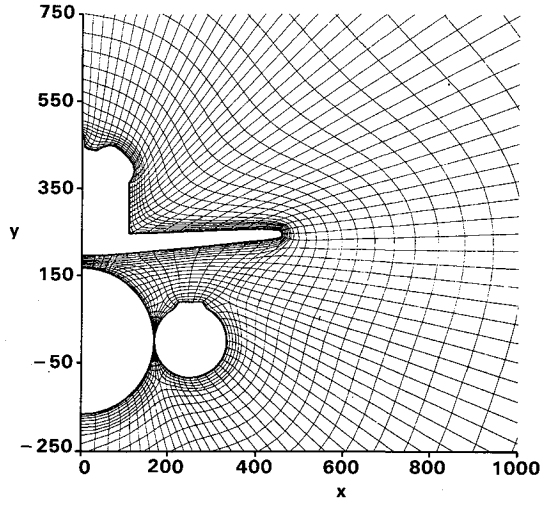

Fig. 2 Example of cross-sectional grid.

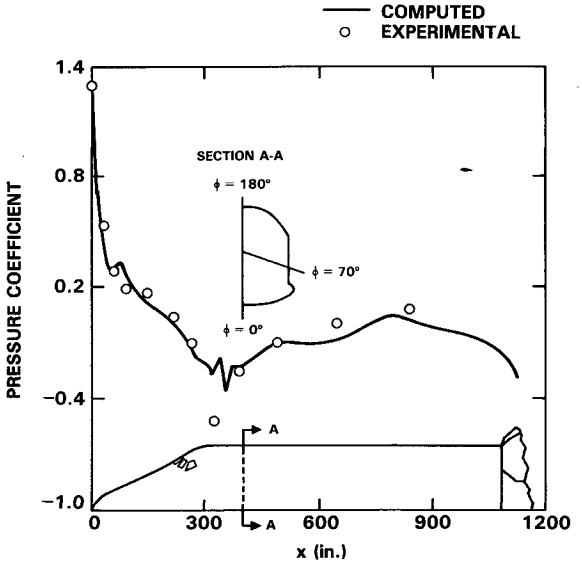

a) $\phi = 70$ deg

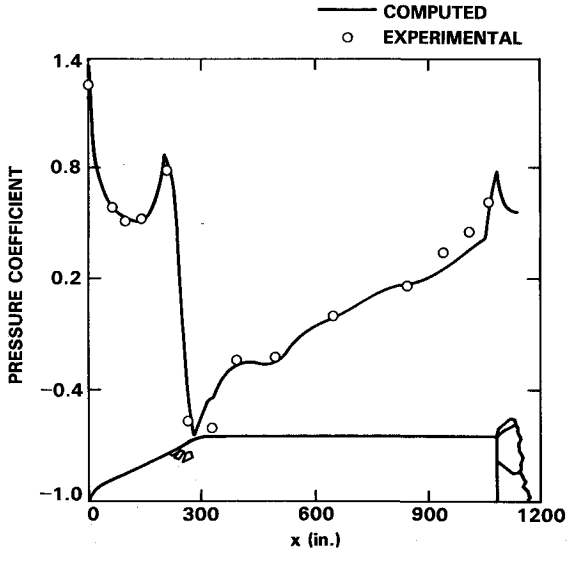

b) $\phi = 180$ deg

Fig. 3 Comparison of pressure distribution with experimental data for two circumferential locations on the Orbiter surface at $M_\infty = 1.05$, $\alpha = -3.0$ deg, and $Re_\infty = 4.0 \times 10^6$/ft; Orbiter alone case.

Table 1 Grid size summary, Orbiter-alone configuration

Grid size	
Range, in.	$\xi \times \eta \times \zeta$
$0 \le X \le 442$	$39 \times 35 \times 40$
$391 \le X \le 1137$	$47 \times 35 \times 64$
$1107 \le X \le 1272$	$47 \times 35 \times 12$

Numerical Scheme

The details of the numerical approach used in the unified solution algorithms (USA) series of codes can be found in Refs. 6 and 7. For the sake of completion, a brief summary of the approach is given here.

The USA series of codes is a very versatile set of codes that can be used to compute numerical solutions to a large class of fluid dynamic problems by solving the Euler or RANS equations. The codes are constructed using a synergistic operational unification of several solution methodologies. They include a mutistage Runge-Kutta explicit scheme, approximate factorization scheme, Gauss-Seidel, and colored relaxation schemes. Underlying these is a common discretization approach based on the total variation diminishing (TVD) formulation using the finite volume framework. The preprocessing approach is used.[6] Various Riemann solvers can be used, with the favorite one being that developed by Roe.[7] A multizone structured grid bookkeeping method facilitates the treatment of complex geometric topologies. In this work, the option of implicit time marching was mainly used, and is described briefly as follows.

The RANS equations integrated over a cell volume and discretized using an implicit method can be represented by

$$\frac{\hat{Q}^{n+1} - \hat{Q}^n}{\Delta\tau} + (\hat{E}_{j+\frac{1}{2}} - \hat{E}_{j-\frac{1}{2}})^{n+1} + (\hat{F}_{k+\frac{1}{2}} - \hat{F}_{k-\frac{1}{2}})^{n+1} + (\hat{G}_{l+\frac{1}{2}} - \hat{G}_{l-\frac{1}{2}})^{n+1} = 0 \tag{1}$$

Here,

$$\hat{Q} = \{e, \rho, \rho u, \rho v, \rho w\}/J$$

where ρ is density; u, v, and w are cartesian velocity components in the x, y, and z directions, respectively; and e is the total energy per unit volume given by $e = p/(\gamma - 1) + \rho(u^2 + v^2 + w^2)/2$ where p is pressure and γ is the ratio of specific heats. Note that J is the Jacobian of the transformation, given by

$$J = \partial(\xi,\eta,\zeta)/\partial(x,y,z)$$

and that j, k, and l are the subscripts associated with the three generalized spatial coordinate directions ξ, η, and ζ; n is the time index; $\Delta\tau$ is the time step; and $\hat{E}$, $\hat{F}$, and $\hat{G}$ are numerical fluxes in the ξ, η, and ζ directions, respectively. These fluxes include both inviscid and viscous flux terms.

The discretized equations are linearized about a known state $Q = q^s$, using a Newton procedure to obtain a better approximation q^{s+1} to Q^{n+1}. Here, s is a subiteration index. Defining

$$\begin{aligned} \Delta^s q &= q^{s+1} - q^s \\ \Delta_j \hat{E} &= \hat{E}_{j+\frac{1}{2}} - \hat{E}_{j-\frac{1}{2}} \\ \Delta_k \hat{F} &= \hat{F}_{k+\frac{1}{2}} - \hat{F}_{k-\frac{1}{2}} \\ \Delta_l \hat{G} &= \hat{G}_{l+\frac{1}{2}} - \hat{G}_{l-\frac{1}{2}} \end{aligned} \tag{2}$$

the Newton procedure can be described by

$$\left[\frac{V}{\Delta\tau} I + \frac{\partial}{\partial q}(\Delta_j \hat{E} + \Delta_k \hat{F} + \Delta_l \hat{G})\right]\Delta^s q = -\left[\frac{V}{\Delta\tau}(q^s - Q^n) + \Delta_j \hat{E}(q^s) + \Delta_k \hat{F}(q^s) + \Delta_l \hat{G}(q^s)\right] \tag{3}$$

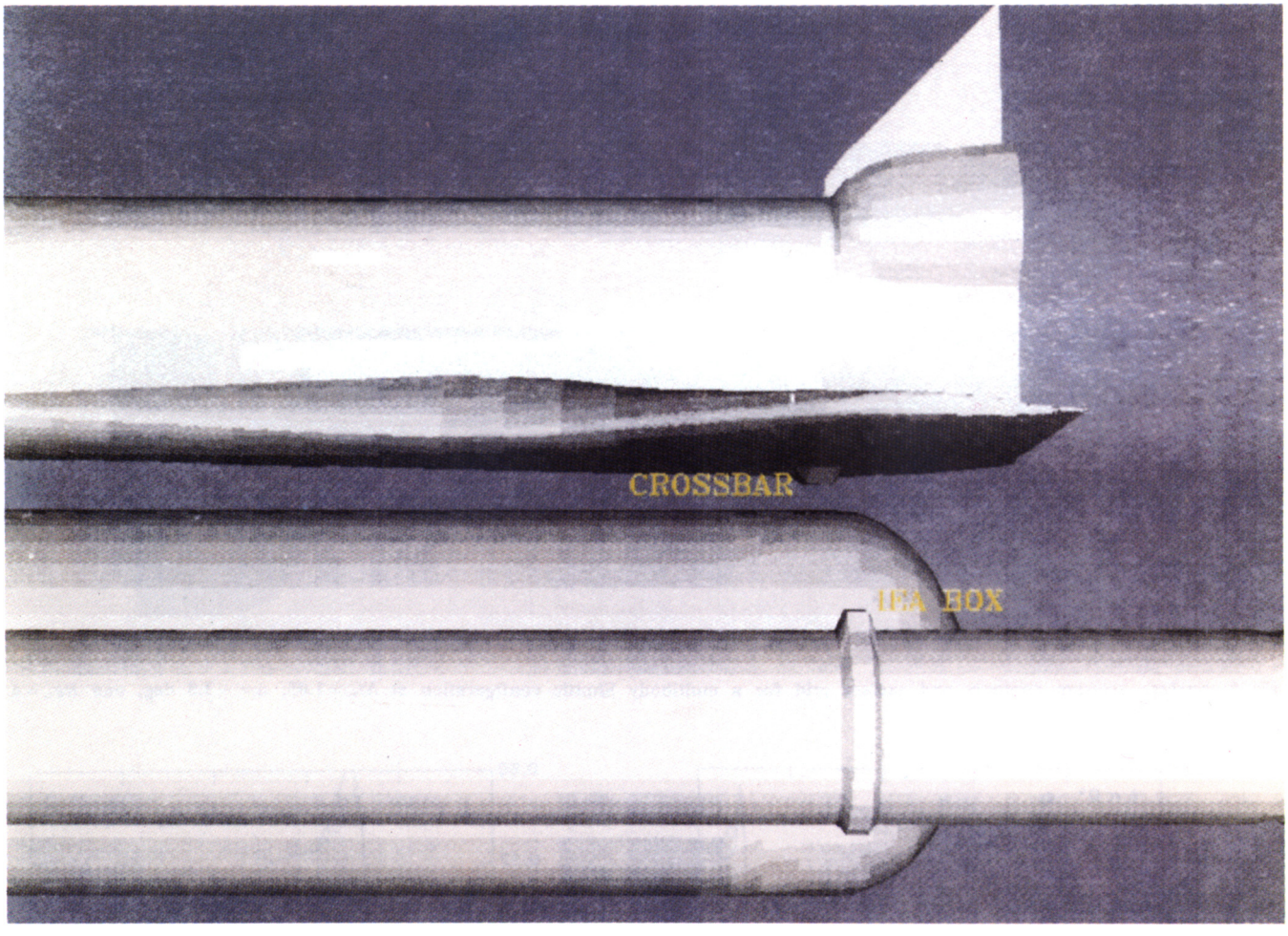

Fig. 4 Location of IEA box with ring and cross bar.

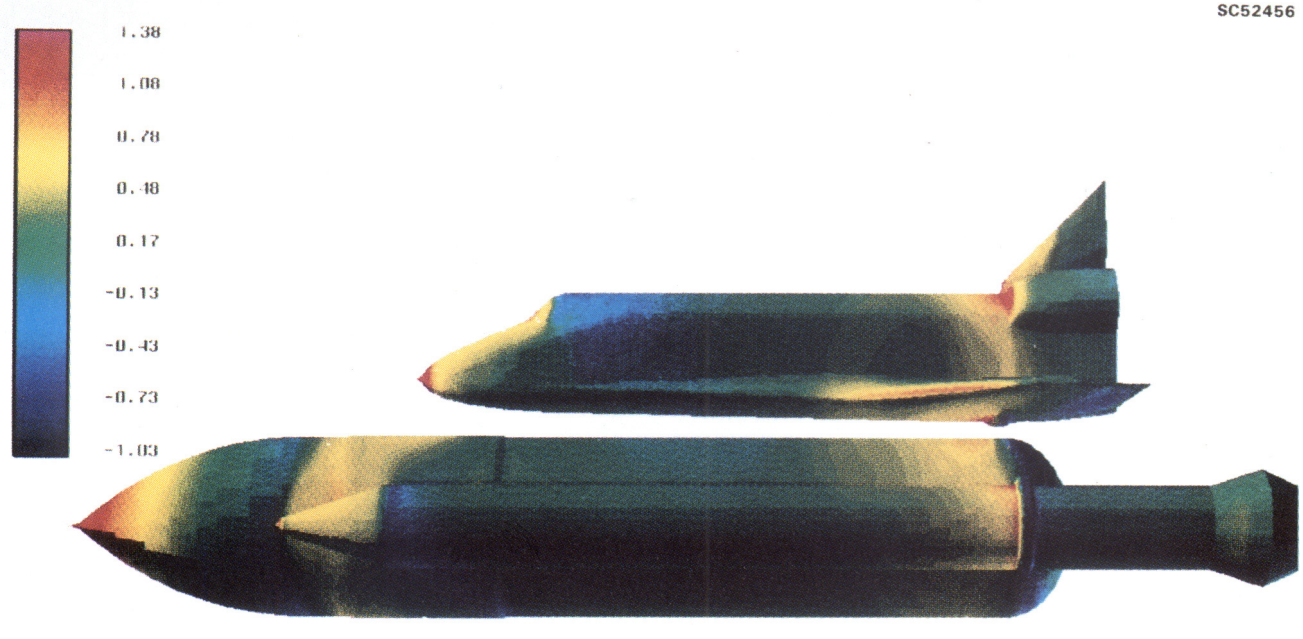

Fig. 5 Surface pressure contours for a multibody Shuttle configuration at $M_\infty = 1.05$, $\alpha = -3.0$ deg, and $Re_\infty = 4.0 \times 10^6$/ft; side view.

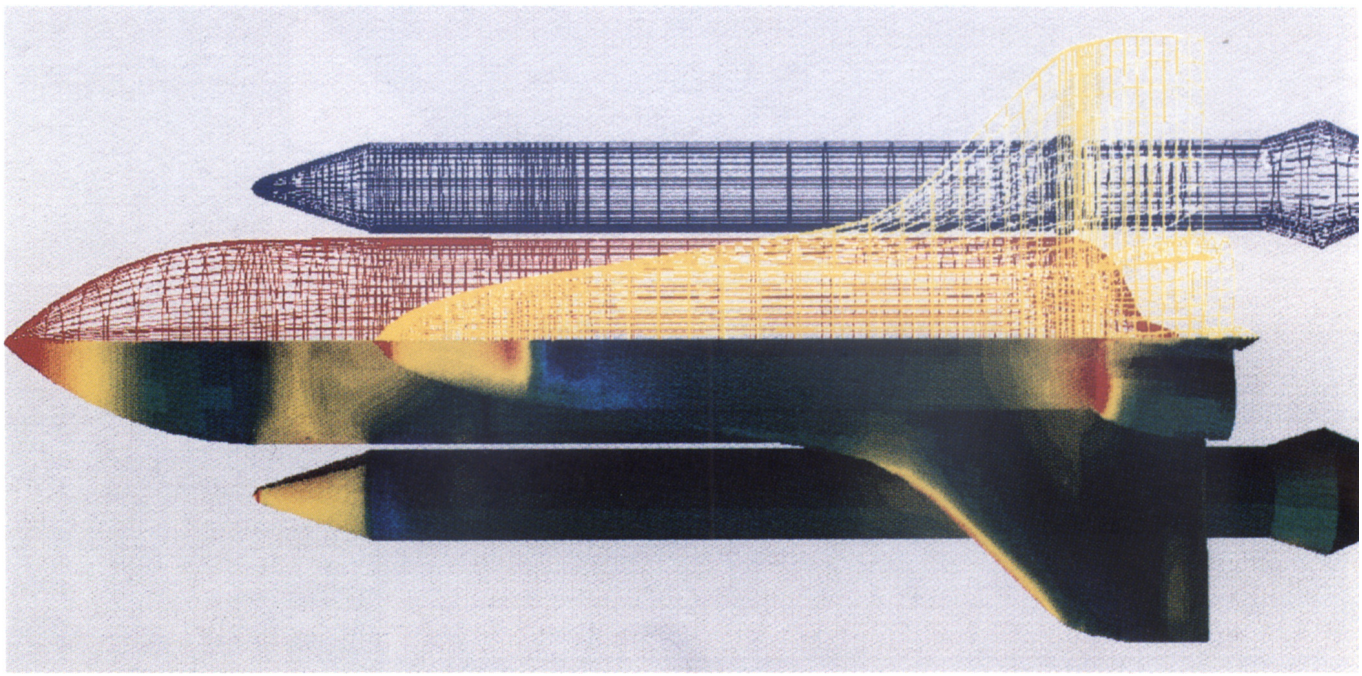

Fig. 6 Surface pressure contours and surface grid for a multibody Shuttle configuration at $M_\infty = 1.05$, $\alpha = -3.0$ deg, and $Re_\infty = 4.0 \times 10^6$/ft; top view.

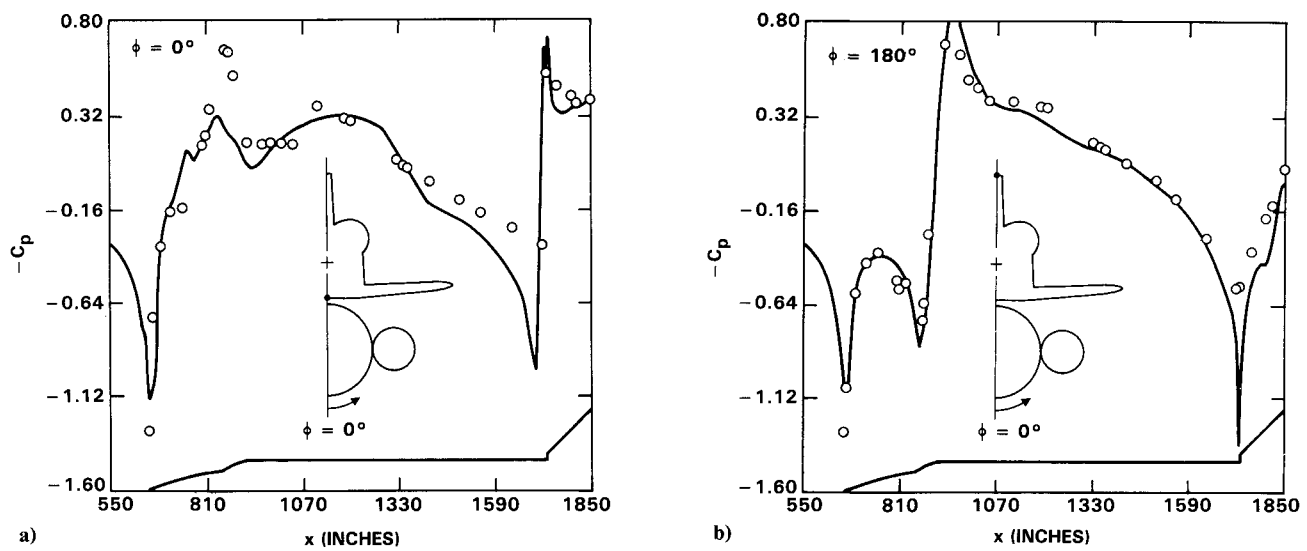

Fig. 7 Comparison for pressure coefficient from computation (-) with experimental data (o) at various locations on the Orbiter surface at $M_\infty = 1.05$, $\alpha = -3.0$ deg, and $Re_\infty = 4.0 \times 10^6$/ft. a) $\phi = 0$ deg, b) $\phi = 180$ deg.

The left-hand side can be simplified by defining an approximation to the true linearization. Toward this goal, we consider only a first-order accurate scheme (based on the first-order numerical flux h) for the left-hand side we include the full high-accuracy scheme on the right-hand side. Even so, when the subiterations converge, the right-hand side is satisfied to the desired tolerance. Next we assume that the eigenvalues and eigenvectors are not functions of q. Using the above, Eq. (3) is simplified to

$$\frac{V}{\Delta\tau}\Delta^s q + A^+_{j-\frac{1}{2}}(\Delta^s q_j - \Delta^s q_{j-1}) + A^-_{j+\frac{1}{2}}(\Delta^s q_{j+1} - \Delta^s q_j)$$
$$+ B^+_{k-\frac{1}{2}}(\Delta^s q_k - \Delta^s q_{k-1}) + B^-_{k+\frac{1}{2}}(\Delta^s q_{k+1} - \Delta^s q_k)$$
$$+ C^+_{l-\frac{1}{2}}(\Delta^s q_l - \Delta^s q_{l-1}) + C^-_{l+\frac{1}{2}}(\Delta^s q_{l+1} - \Delta^s q_l)$$
$$= \text{right-hand side of Eq. (3)} \qquad (4)$$

where

$$A^\pm_{j\pm\frac{1}{2}} = R_{j\pm\frac{1}{2}}\Lambda^\pm_{j\pm\frac{1}{2}}L_{j\pm\frac{1}{2}}$$
$$B^\pm_{k\pm\frac{1}{2}} = R_{k\pm\frac{1}{2}}\Lambda^\pm_{k\pm\frac{1}{2}}L_{k\pm\frac{1}{2}}$$
$$C^\pm_{l\pm\frac{1}{2}} = R_{l\pm\frac{1}{2}}\Lambda^\pm_{l\pm\frac{1}{2}}L_{l\pm\frac{1}{2}} \qquad (5)$$

Here,

$$\Lambda^\pm = (\Lambda \pm |\Lambda|)/2 \qquad (6)$$

where Λ is the diagonal matrix whose diagonal elements are λ^i and $|\Lambda|$ is the diagonal matrix whose diagonal elements are $|\lambda^i|$. These equations, together with the appropriate boundary conditions, are solved using the well-known method of approximate factorization.

Table 2 Grid size summary, multibody Shuttle configuration

Zone no.	Grid size $\xi \times \eta \times \zeta$
1	$52 \times 15 \times 103$
2	$35 \times 15 \times 103$
3	$39 \times 11 \times 103$
4	$10 \times 10 \times 103$
5	$76 \times 21 \times 103$

Boundary Conditions

The USA series of codes allows specification of pointwise boundary conditions. All the boundary conditions in the codes are imposed with calls to modular routines. In the case of flow past the multibody Shuttle, the boundary conditions are as follows:

1) Adiabatic, no-slip condition at solid walls;
2) Freestream condition at the inflow boundary;
3) Nonreflective characteristic boundary condition at the boundary far away from the bodies (far-field boundary);
4) Zeroth order extrapolation for the outflow boundary;
5) Zero flux condition on the plane of symmetry;
6) Zonal boundary condition to ensure continuity of flow variables across the zonal boundaries and to maintain the same stencil as for interior cells; and
7) Inviscid wall condition for simulating the orbiter and the SRB plumes.

Grid Generation

The geometry of the configuration is prescribed at discrete points in a cross plane (x = const plane) at various axial locations. The cross section perimeter is divided into a number of patches, each of which is splined to create a continuous surface definition. Then, the point distribution for each patch is calculated based on the clustering requirements and the computed spline coefficients. Because each patch is splined separately, surface slope discontinuities can be modeled accurately by placing patch end points at the locations of discontinuity. The series of patches for each cross section describes the configuration surface. The number of patches used can vary from cross section to cross section.

In the case of the Orbiter alone, only one zone is required to generate an elliptic grid for the entire flowfield (Fig. 1a). Several patches are used to properly represent all the slope discontinuities on the surface of the Orbiter.

In the case of the multibody Shuttle, the whole flowfield is divided into five zones at each cross section; one inner zone to capture viscous flow effects around each of the three bodies, namely, the Orbiter, the external tank, and the solid rocket booster; one interaction zone in the region below the Orbiter's wing; and an outer zone (Fig. 1b). The two-dimensional grids generated at each cross section using an elliptic solver (see Ref. 5 for details) are stacked up in the nose-to-tail direction. The inter-zonal boundaries are obtained as part of the grid generation procedure. The initial shape of the inter-zonal boundaries is specified quite arbitrarily, and the initial guesses for the interior points are obtained from the boundary points using an algebraic interpolation. An example of a crossplane grid is shown in Fig. 2. Across the zonal boundaries, the grid lines are continuous and the mesh sizes are fairly continuous.

Results and Discussion

Some geometric simplifications were introduced to reduce the complexity of the numerical simulation. The actual mated Space Shuttle geometry is so complex that it is very difficult to completely simulate the exact geometry either in a wind tunnel or in a numerical computation. Luckily, such an exact simulation is probably not critical for the purpose of evaluating aerodynamic loads. However, it is indeed important to ensure that any simplification introduced in the geometry of a component does not alter its blockage significantly. This point will be discussed later in this section.

Two flight conditions that correspond to the Space Shuttle vehicle in ascent mode were chosen for numerical simulation. They are 1) $M_\infty = 1.05$, $\alpha = -3.0$ deg, and $Re_\infty = 4.0 \times 10^6$/ft; and 2) $M_\infty = 1.25$, $\alpha = -2.2$ deg, and $Re_\infty = 3.6 \times 10^6$/ft.

These flight conditions were chosen because wind-tunnel measurement have been carried out for them, so that they can serve as test cases for evaluation of the performance of numerical simulations. All the results shown here were computed using the USA code's zero equation turbulence model.[8] For the purpose of computing the overall attached flowfield (neglecting local small-scale separation and the base flow region) and predicting mean flow quantities such as pressure, this simple turbulence model may be sufficient.

Orbiter Alone

Calculation were carried out for $M_\infty = 1.05$, $\alpha = -3$ deg, and $Re_\infty = 4.0 \times 10^6$/ft. The grid size is summarized in Table 1. The nose of the orbiter is at $X = 0.0$. The grid was divided into three sections with overlapping regions. Time marching was used to obtain a reasonably converged solution in section one. With the solution at $X = 442$ in. as the initial solution, a space

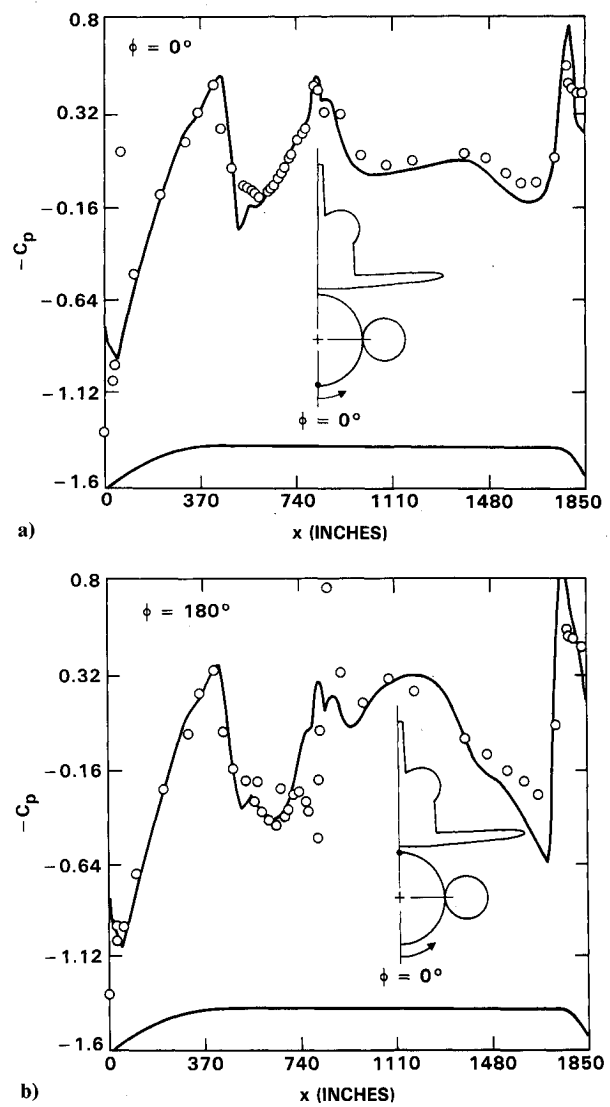

Fig. 8 Comparison of pressure coefficient from computation (-) and experimental data (o) at various locations on the external tank surface at $M_\infty = 1.05$, $\alpha = -3.0$ deg, and $Re_\infty = 4.0 \times 10^6$/ft. a) $\phi = 0$ deg, b) $\phi = 180$ deg.

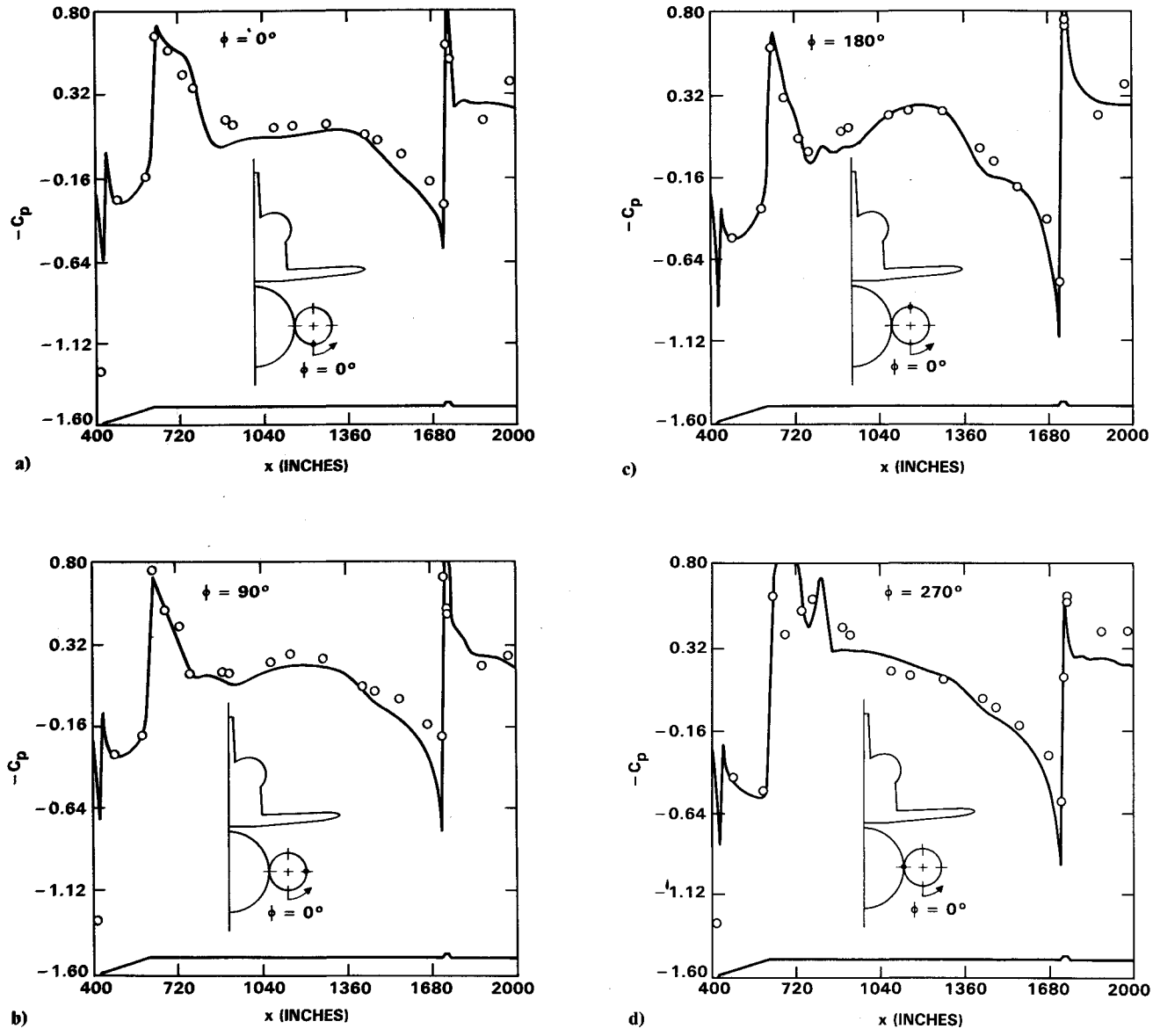

Fig. 9 Comparison of pressure coefficient from computation (-) and experimental data (o) at various locations on the solid rocket booster surface at $M_\infty = 1.05$, $\alpha = -3.0$ deg, and $Re_\infty = 4.0 \times 10^6$/ft. a) $\phi = 0$ deg, b) $\phi = 90$ deg, c) $\phi = 180$ deg, d) $\phi = 270$ deg.

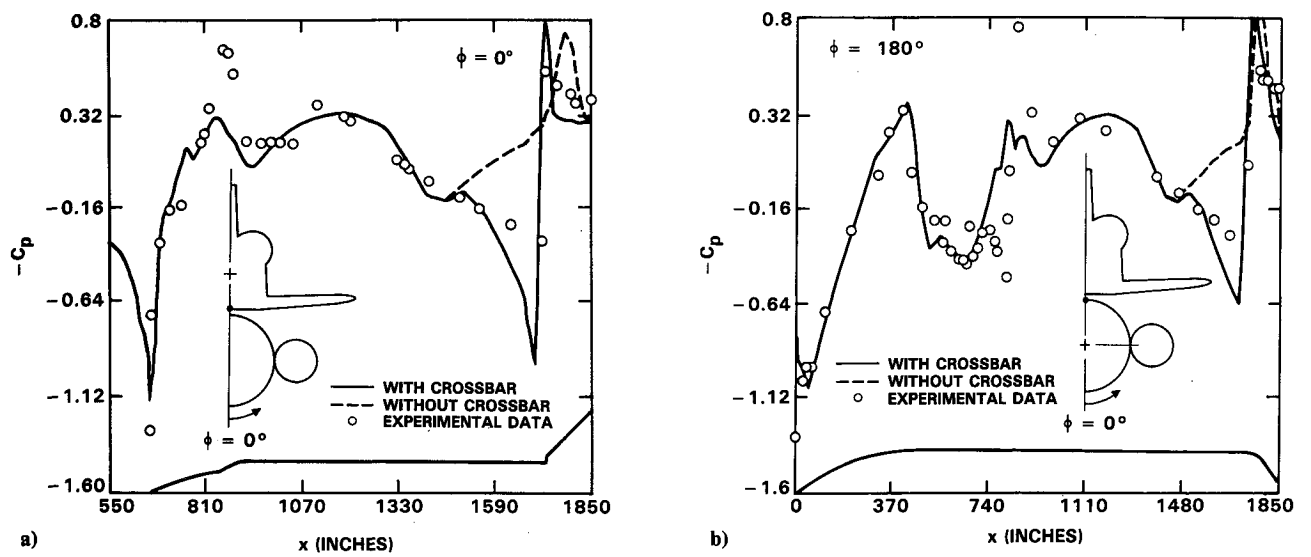

Fig. 10 Crossbar effects on surface pressure distribution at $M_\infty = 1.05$, $\alpha = -3.0$ deg, and $Re_\infty = 4.0 \times 10^6$/ft. a) $\phi = 0$ deg, b) $\phi = 180$ deg.

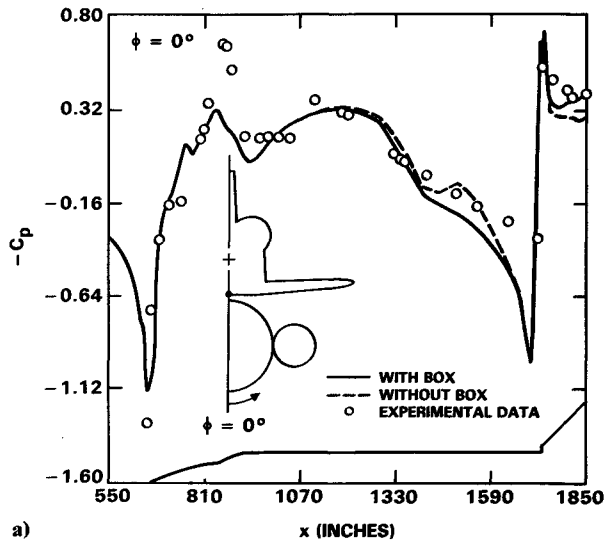

a)

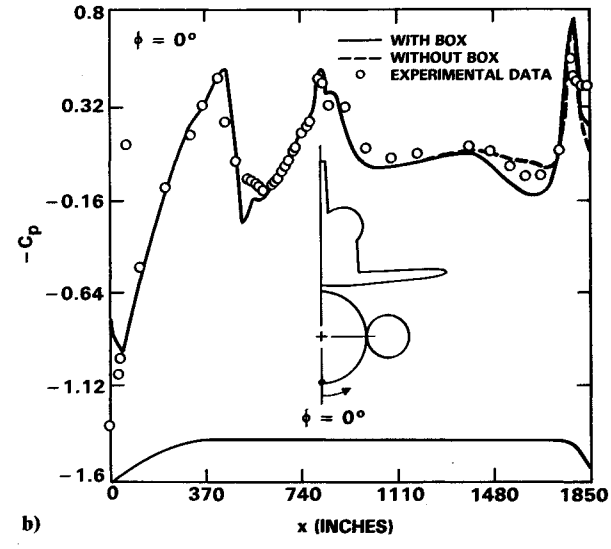

b)

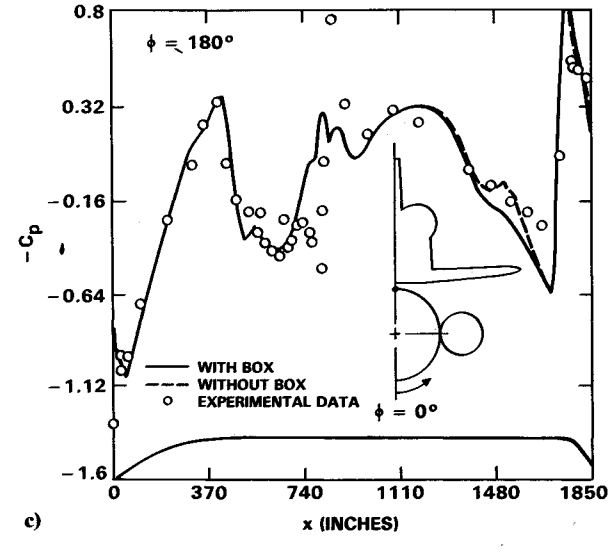

c)

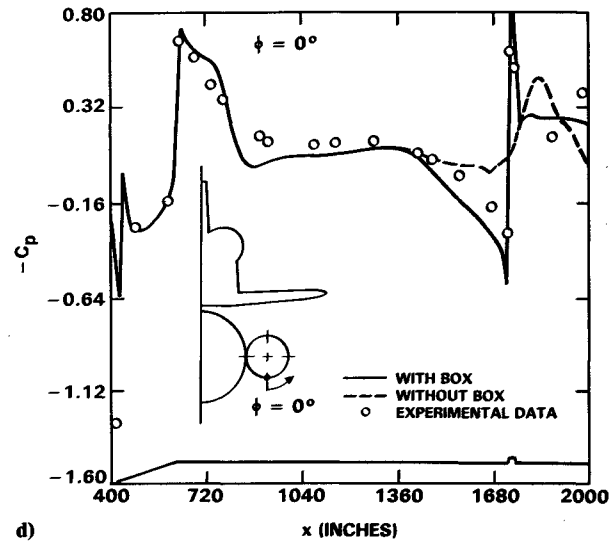

d)

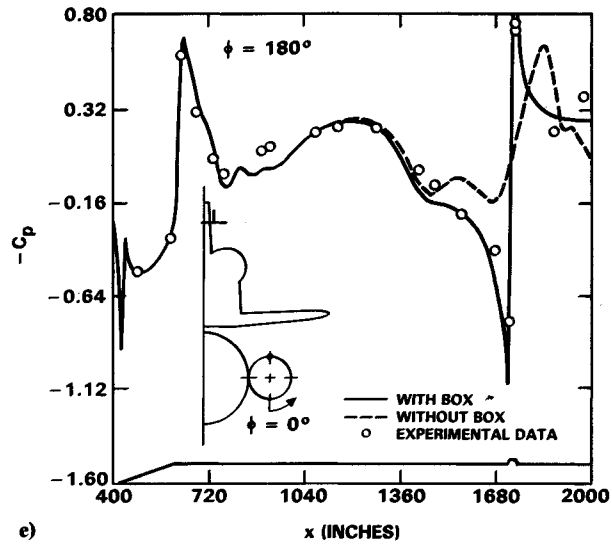

e)

Fig. 11 IEA box effects on surface pressure distribution at $M_\infty = 1.05$, $\alpha = -3.0$ deg, and $Re_\infty = 4.0 \times 10^6$/ft. a) $\phi = 0$ deg on Orbiter, b) $\phi = 0$ deg on external tank, c) $\phi = 180$ deg on external tank, d) $\phi = 0$ deg on solid rocket booster, e) $\phi = 180$ deg on solid rocket booster.

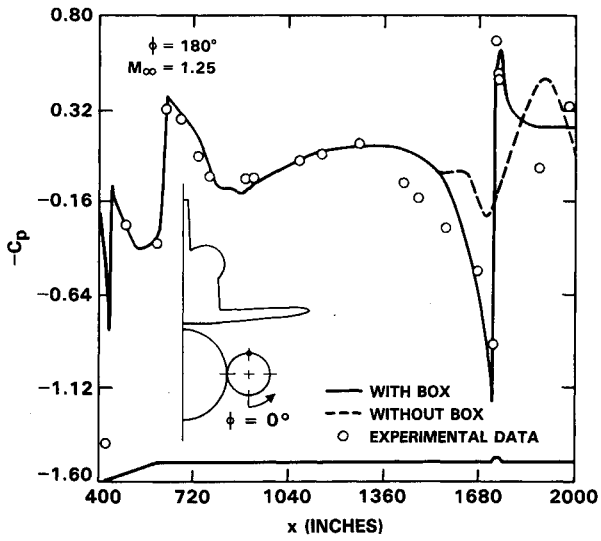

Fig. 12 IEA box effects on surface pressure distribution at $M_\infty = 1.25$, $\alpha = -2.2$ deg, and $Re_\infty = 3.6 \times 10^6$/ft.

marching technique was used to obtain a good initial guess for the flowfield in the downstream, so that only about 300 time iterations were then required to reach convergence. The results obtained from this calculation are compared with experimental measurements in Fig. 3. The wiggle in the pressure distribution for $\phi = 70$ deg (Fig. 3a) near $X = 300$ in. is caused by an error in the definition of the geometry that was originally given to us. The error was subsequently corrected for the multibody Shuttle case.

Multibody Shuttle Configuration

One of the main problems of interest in the study of flow past the mated Shuttle vehicle is the evaluation of the effect of protuberances like the forward and aft attachments (e.g., cross bar, thrust strut, and vertical strut), fuel lines, and the integrated electronics assembly (IEA) box with ring, on the aerodynamic loads. Such a study should help improve the design of the protuberances and eventually result in an increase in efficiency of the Shuttle missions.

Here we study the effect of two such protuberances, namely, the IEA box with ring mounted on the SRB and the cross bar under the Orbiter (Fig. 4). We present results for three configurations: 1) without either cross bar or IEA box, 2) with cross bar but without IEA box, and 3) with both cross bar and IEA box. The first two cases are useful in evaluating the effect of the cross bar, and the last two enable us to calculate the increase in wing loading caused by the presence of the IEA box.

The first case considered here is for $M_\infty = 1.05$, $\alpha = 3$ deg, and $Re_\infty = 4.0 \times 10^6$/ft. The grid size is summarized in Table 2. The grid density is sufficiently fine in the direction normal to the wall (η direction in Fig. 1) to resolve the turbulent boundary layer on all three bodies. Even the circumferencial grid spacing (ξ) appears to be reasonable. On the other hand, the axial grid spacing needs refinement in some locations to resolve more accurately some of the flow features, such as that due to the leading edges of the wings. The cross bar was modeled by a $27 \times 96 \times 7$ in. hexahedral bump attached to the Orbiter. The exact shape and size of the cross bar were not available to us at the time of this computation. (Forward attach hardware, thrust strut, feedline blockage, elevon deflection, and vertical strut are not included in the present work.)

Initially, the grid was divided into two regions to satisfy the memory constraints of the CRAY YMP at NASA Ames Research Center. The first region had 68 axial locations and the second 44, with an overlap of 9 X locations. The extent of the first region was arrived at from a coarser grid computation (only 28 axial stations). The last axial station of the first region was chosen such that the flow outside the boundary layer was supersonic at that location. This is an important requirement for fast convergence, since initially only the first region is solved for with supersonic outflow boundary condition imposed on the last plane. Overlapping of the two regions is another factor in accelerating the convergence rate. After reasonably converged solutions for the two regions were obtained by solving them separately, the two regions were combined to form a single continuous region and a few more time iterations were carried out on the CRAY 2 to obtain the final converged solution. The total number of iterations was about 1000.

The results of the third configuration are shown in Figs. 5–9. Surface pressure contours and surface grid of the multibody Shuttle are shown in Figs. 5 and 6, and the pressure coefficients at various axial locations are compared with experimental data in Figs. 7–9. The nose of the ET is location at $X = 0.0$. Generally speaking, the comparison between computed and measured pressures is reasonable. Some local discrepancy can be found due to lack of modeling of some of the components and insufficient grid resolution. For instance, local effects of the forward attach hardware can be seen in Figs. 7 and 8 near $X = 810$ in. Also, the difference between measured and computed pressures in the region 1300 in. $\leq X \leq 1600$ in. could be attributed to the incomplete definition of the aft attach hardware in the numerical model.

The present results also agree well with the calculation in Ref. 3, which is not included here. Furthermore, there are some improvements in the expansion region with the present approach. The results in Ref. 3 were obtained using the chimera grid scheme with more than twice the amount of grid points.

The results of the first and second configurations are compared in Fig. 10. The effects of the simplified crossbar model are shown. The simplified model could predict correct local compression trend, whereas without the crossbar model the numerical simulation predicts an expansion in this region.

By comparing the results of the second and third configurations, the effect of the IEA box with ring on the pressure distribution is shown in Fig. 11. The box causes a large compression and the shock wave even impinges on the lower surface of the wing. The results with the box agree better with experimental data than those without it. All these results demonstrate that we can obtain a better solution if we have enough geometry information and, also, that the USA series code can handle very complex geometries with reasonable accuracy and ease.

For the same geometry model, another calculation was carried out for flight conditions $M_\infty = 1.25$, $\alpha = 2.2$ deg. The effects of the IEA box are again shown in Fig. 12. Further improvements in comparison with data require a complete modeling of the aft attach hardware, elevon deflection, and, possibly, a finer grid too.

Concluding Remarks

A numerical simulation of the multibody Shuttle has been carried out using a multizonal approach. The calculations agree reasonably well with experimental data for the pressure field. The interference effects of various components on the surface are discussed. The effects of the IEA box and the cross bar on the pressure distribution are shown. Based on this work, it can be expected that a refined geometry definition will further improve the solution quality.

References

[1]Szema, K. Y., Chakravarthy, S. R., Riba, W. T., Byerly, J., and Dresser, H. S., "Multi-Zone Euler Marching Technique for Flow over Single and Multi-Body Configurations," AIAA Paper 87-0592, Jan. 1987.

[2]Szema, K. Y., Charkravathy, S. R., Pan, D., Bihari, B. L., Riba, W. T., Akdag, V. M., and Dresser, H. S., "The Application of a Unified Marching Technique for Flow over Complex 3-Dimensional Configurations Across the Mach Number Range," AIAA Paper 88-

0276, Jan. 1988.

[3]Buning, P. G., Chiu, I. T., Obayashi, S., Rizk, Y. M., and Steger, J. L., "Numerical Simulation of the Integrated Space Shuttle Vehicle," AIAA Paper 88-4359, Aug. 1988.

[4]Steger, J. L., Dougherty, F. C., and Benek, J. A., "A Chimera Grid Scheme," *Advances in Grid Generation*, edited by K. N. Ghia and U. Ghia, American Society of Mechanical Engineers, ASME FED-5, New York, 1983, pp. 59-69.

[5]Rajagopal, K., Szema, K. Y., Ramakrishnan, S., Chen, C. L., and Lick, W. J., "A Versatile Multi-Zonal Gridding Technique For Complex Geometries," AIAA Paper 90-0011, Jan. 1990.

[6]Chakravarthy, S. R., and Osher, S., "Computing with High-Resolution Upwind Schemes for Hyperbolic Equations," *Proceedings of 1983 AMS-SIAM Summer Seminar on Large-Scale Computations in Fluid Mechanics*, Vol. 22, Lectures in Applied Mathematics, American Mathematical Society, 1985.

[7]Chakravarthy, S. R., Szema, K. Y., and Haney, J. W., "Unified 'Nose-to-tail' Computational Method for Hypersonic Vehicle Applications," AIAA Paper 88-2564, June 1988.

[8]Ramakrishnan, S., Goldberg, U., and Ota, D., "Numerical Computation of Hypersonic Turbulent Flows Using Zero and One Equation Models," AIAA Paper 89-2234, July 1989.

Walter B. Sturek
Associate Editor